Study of the Interface in a GaP/Si Heterojunction Solar Cell

Rebecca Saive, Hal Emmer, Christopher T. Chen, Chaomin Zhang, Christiana Honsberg, and Harry Atwater

***Abstract*—We have investigated the GaP/Si heterojunction interface for application in silicon heterojunction solar cells. We performed X-ray photoelectron spectroscopy (XPS) on thin layers of GaP grown on Si by metal organic chemical vapor deposition and molecular beam epitaxy. The conduction band offset was determined to be 0.9 $\pm$ 0.2 eV, which is significantly higher than predicted by Anderson's rule (0.3 eV). XPS also revealed the presence of Ga–Si bonds at the interface that are likely to be the cause of the observed interface dipole. Via cross-sectional Kelvin probe force microscopy (*x*-KPFM), we observed a charge transport barrier at the Si/GaP interface which is consistent with the high-conduction band offset determined by XPS and explains the low open-circuit voltage and low fill factor observed in GaP/Si heterojunction solar cells.**

***Index Terms*—Band alignment, interface, Kelvin probe (KP) force microscopy, silicon heterojunction (SHJ) solar cells, X-ray photoelectron spectroscopy.**

I. Introduction

DESPITE the maturity of silicon solar cells, careful materials and photonic design have led to recent efficiency improvements, with a current record efficiency of over 26.0% achieved by Kaneka [1]. This record solar cell uses a silicon heterojunction [2] material stack that features high-purity crystalline silicon as an absorber material, intrinsic amorphous silicon ((i) a-Si) passivation, and doped a-Si as carrier selective contacts. This approach leads to low recombination losses and, therefore, to record high open-circuit voltages. Furthermore, the record solar cell uses an interdigitated back contact (IBC) design that enables all electrical contacts to connect to the back of the solar cell, mitigating optical losses from reflection on metallic front contacts and parasitic absorption in transparent conductive oxides. However, the IBC approach is sophisticated and expensive, and a high efficiency, front-contacted heterojunction solar cell would be preferable for large-scale lower cost manufacturing. Furthermore, IBC solar cells cannot be used as bifacial solar cells [3], [4]. Therefore, extensive effort has been made to develop high-efficiency silicon heterojunction solar cells with selective contacts on the rear and front sides [5], [6]. Although reflection losses on front electrodes can be mitigated by using effectively transparent contacts [7]–[9], there exist inherent disadvantages of using a-Si as a selective contact: 1) a-Si exhibits high parasitic absorption, leading to a decrease in short-circuit current density (Jsc); 2) the conductivity of a-Si is too low for efficient lateral charge transport, necessitating the use of a transparent conductive oxide (TCO) layer. The TCO—usually indium tin oxide (ITO)—also parasitically absorbs and leads to further Jsc decrease. The Jsc losses within the amorphous Si and the ITO add up to 2.6 mA/cm^2 [10]. These losses could potentially be avoided by replacing a-Si with high band gap, high mobility materials. Recently, several materials have been proposed and integrated [6], [11]–[14]. GaP appears to be a promising candidate as its large indirect band gap (2.26 eV [15]) would ensure low parasitic absorption. Furthermore, based upon the accepted electron affinity values for Si (4.05 eV [16]) and GaP (3.8 eV [16]) Anderson's rule suggests a high theoretical valence band offset (0.89 eV) and low-conduction band offset (0.25 eV). Given these assumptions, GaP should provide excellent hole blocking and selective electron extraction properties. A schematic of the proposed device scheme is shown in Fig. 1. Simulations predict an open-circuit voltage (V_{OC}) of 710 mV for a Si/GaP solar cell [17]. However, at most real interfaces, Anderson's rule fails due to Fermi-level pinning [18] and interface dipoles [18]–[21]. Therefore, experimentally reported solar cell properties

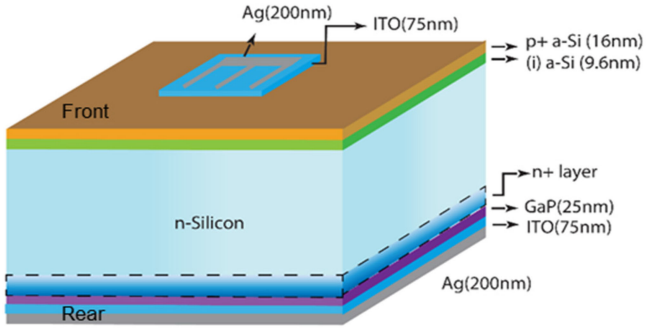

Fig. 1. Schematic of a silicon heterojunction solar cell with conventional (i) a-Si/p+ a-Si front selective contact and the MBE-grown GaP rear selective contact.

Manuscript received May 15, 2018; revised June 27, 2018; accepted July 25, 2018. Date of publication August 13, 2018; date of current version October 26, 2018. This work was supported in part by the U.S. Department of Energy, Energy Efficiency and Renewable Energy Program, under Award No. DE-EE0006335 for band offset characterization and in part by the U.S Department of Energy and the National Science Foundation under grant EEC1041895 for other electrical and structural measurements and in part by the Molecular Foundry funded by the Office of Science, Office of Basic Energy Sciences, U.S. Department of Energy under Contract DE-AC02-05CH11231. *(Corresponding author: Rebecca Saive.)*

R. Saive, H. Emmer, C. T. Chen, and H. Atwater are with the California Institute of Technology, Pasadena, CA 91125 USA (e-mail: r.saive@utwente.nl; hal.emmer@gmail.com; christopherchen@lbl.gov; haa@caltech.edu).

C. Zhang and C. Honsberg are with the Arizona State University, Tempe, AZ 85287-5706 USA (e-mail: Chaomin.Zhang@asu.edu; Christiana.Honsberg@asu.edu).

Color versions of one or more of the figures in this paper are available online at http://ieeexplore.ieee.org.

Digital Object Identifier 10.1109/JPHOTOV.2018.2861724

[22]–[24] significantly deviate from the theoretical predictions [17], [25], [26]. In order to understand this discrepancy, the underlying physics of interface band structure and carrier transport needs to be understood. Most notably, the fill factor of devices that use GaP as one of the selective contacts is very low and in the case of our devices even S-shaped current–voltage characteristics are observed. S-shaped current–voltage characteristics are a common phenomenon in silicon heterojunction solar cell research [6], [27]–[30] and often are attributed to barriers for charge carrier extraction caused by unfavorable band alignment [6], [28]. We found in our devices that the S-shaped characteristics disappear and a higher fill factor is obtained when highly n-doping the silicon at the interface with GaP. This suggests that the conduction band offset is much higher than expected from Anderson's model, which leads to barriers in charge transport [6], [28], [31] and therefore, S-shaped current–voltage characteristics [6], [27]–[31]. The properties of the GaP/Si interface and the real band alignment at the GaP/Si interface have been widely discussed in the literature in experimental [32]–[40] and theoretical studies [41]–[44]. For instance Perfetti *et al.* found as valence band offset 0.8 ± 0.1 eV [33] and 0.66 ± 0.1 eV [39], Katnani *et al.* reported 0.95 ± 0.1 eV [40], and Niles and Höchst measured 0.53 eV [32]. The large spread in reported band alignment values most likely results from a strong dependence of the interface properties on the fabrication method. In many reports, Si was grown on GaP. For using in silicon heterojunction solar cells, GaP is epitaxially grown on high carrier lifetime silicon, so it is of considerable interest to investigate the band alignment for GaP/Si heterojunctions in which GaP is grown on Si—in our case by organometallic vapor phase epitaxy and molecular beam epitaxy. Recently, this topic has gained momentum, and several reports on different preparation techniques and the resulting interface properties have been published [22], [23], [34], [38], [44], [45].

Here, we report on an experimental investigation to determine the band alignment at the GaP/Si heterojunction interface, with GaP grown using methods similar to those which could be employed in a solar cell fabrication process. We present an extensive X-ray photoelectron spectroscopy (XPS), Kelvin probe (KP) [46], and cross-sectional KP force microscopy (KPFM) [47]–[51] study of GaP grown on high-carrier lifetime silicon by metalorganic chemical vapor deposition (MOCVD) and molecular beam epitaxy (MBE). We found that the conduction band offset is significantly higher than predicted by the Anderson model, which provides a possible explanation for the observed device characteristics. We compare our results to the literature and discuss explanations for discrepancies.

II. Sample Preparation

GaP was grown by MBE and MOCVD on Si (0 0 1) with a 6° offcut [45] and (1 1 2) [52] orientation. In order to suppress charge carrier lifetime degradation [53] during the GaP growth, the samples were protected with PECVD SiN_x on their back sides [54], [55].

A. Molecular Beam Epitaxy

MBE growth was performed on 270-μm-thick Si wafers with a resistivity of 3 Ω·cm resulting from phosphorous doping at a density of about 5×10^{15} cm^{-3}. n+ doping was achieved by phosphorous diffusion in a $POCl_3$ furnace at 830 °C [56] and yielded a sheet resistance of the n+ layer of 30 Ω/sq. GaP of 25 nm with nominal 10^{18} cm^{-3} Si doping was epitaxially grown on the Si at 580 °C via MBE with a P/Ga ratio of ~4.5. At the initiation of the growth, the P shutter was open for 20 s for P deposition. Then, ten short-period loops of (GaP-P) with 5-s GaP deposition and 5 s pause under P-flux were applied to improve the planarity of the grown surface for the subsequent main growth process. After GaP deposition, SiN_x layers were removed by concentrated HF, and the n + layer on the back was etched off by a mixture of HNO_3:HF:CH_3COOH. The charge carrier lifetime of Si was confirmed to be more than 500 μs [53]–[55]. As depicted in Fig. 1(a), intrinsic a-Si and p+ a-Si layers were deposited by PECVD, and ITO and Ag were sputtered to form an electrical front contact. Fig. 1(a) shows a systematic drawing of the final solar cell device structure.

B. Metalorganic Chemical Vapor Deposition

Furthermore, GaP was epitaxially grown on Si with (0 0 1) [45] and (1 1 2) orientation by MOCVD in a heavily modified Thomas Swan Epitor II with a close coupled showerhead. We used Si (0 0 1) 6° offcut toward [1 1 1] from ITME, Czochralski grown and Boron doped with resistivity of 4–6 Ω·cm corresponding to a doping level of around 3×10^{15} cm^{-3}. Si (1 1 2) was obtained from Semiconductor Processing, Co., float zone grown and Boron doped with resistivity >5000 Ω·cm and, therefore, a doping level of around 2×10^{12} cm^{-3}. We chose Si (0 0 1) 6° offcut toward [1 1 1] and Si (1 1 2) as both these crystal orientations are known to prevent antiphase domains [57]. Substrates were cleaned with water, acetone, and isopropanol in an ultrasonic bath for 10 min, respectively. Afterward, organic contaminants were removed by a 10-min ozone treatment. Subsequently, the native oxide was removed by a 2 min dip in 5% hydrofluoric acid. The transfer from the HF bath to inert atmosphere was performed in less than 5 min in order to limit the formation of new native oxide. Cross-sectional transmission electron microscopy images do not show any evidence of oxygen contamination [58]. All growth was performed at 100 mbar reactor pressure with hydrogen carrier gas. The metalorganic precursors used were triethylgallium (TEGa, 63 μmol/min) and tertiarybutylphosphine (TBP, 3205 μmol/min^{-1}) [59]. The first layers were grown layer by layer in an atomic layer epitaxy (ALE) process [45], [60] at 450 °C to ensure high-quality nucleation layers. Contrary to conventional MOCVD, in an ALE process the two precursor gases are not offered at the same time but in short alternating pulses (5 s for TEGa, 10 s for TBP). Thin films with thicknesses smaller or in the range of the photoelectron escape depth (~10 nm) were exclusively grown by ALE with a growth rate of 1 nm/min. Thicker layers were obtained by a subsequent conventional MOCVD growth at 590 °C with a growth rate of 20 nm/min. The ALE growth was initiated by TBP. However, Beyer *et al.* found that the first bond that Si forms is with Ga due to the poor decomposition of TBP [61] and Supplie *et al*. [38] found that Si–Ga nucleation occurs before the first nucleation pulse, as outgassing from the reactor walls supplies Ga and P species to the substrate surface before the

intended start of growth. The GaP was not intentionally doped, but we can deduce light n-type background doping as XPS peaks of thicker layers shift toward higher binding energy (as shown in Fig. 3). Layer thicknesses were determined via X-ray reflectometry [58]. Antiphase domains were identified when grown on Si (0 0 1) 6° offcut toward [1 1 1], however, GaP thin films grown on Si (1 1 2) do not reveal any evidence of antiphase domains [58]. This was determined by comparing cross-sectional transmission electron microscopy and atomic force microscopy results with literature findings [58]. Charge carrier lifetimes in the Si of up to 75 μs were achieved with ALE grown GaP on Si similar to other growth studies [62].

III. Measurement Methods

A. X-Ray Photoelectron Spectroscopy

XPS measurements were performed with a Kratos Ultra XPS or an M-Probe ESCA/XPS. An Al Kα (1.486 keV) monochromatic X-ray source was used in both instruments. After growth, samples were stored under nitrogen atmosphere and briefly (5–20 min) exposed to ambient air while being transferred to the XPS vacuum system. In order to obtain good signal-to-noise ratio, core-level measurements were integrated over 30 scans and valence band measurements were integrated over 100 scans with the M-Probe ESCA/XPS and 35–50 scans with the Kratos Ultra XPS. With the Kratos Ultra XPS, the pass energy of the analyzer was 10 eV and with the M-Probe ESCA/XPS 20 eV. The integration time per scan was 100 ms and the step size 0.025 eV for both instruments. This leads to an energy resolution of ~0.8 eV for the M-Probe ESCA/XPS and ~0.3 eV for the Kratos Ultra XPS.

In XPS measurements, the difference between the valence band onset and the core level peaks stays constant [63], and therefore, a change in the core-level position implies the same change in the valence band position. Using this correlation, we can derive the valence band offset ΔE_V at the interface by

$$\Delta E_V = \Delta E_{\mathrm{CoreLevel-Valence}}\ (\text{thick GaP}) - \Delta E_{\mathrm{CoreLevel-Valence}}\ (\text{bare Si}) - (\mathrm{BE_{GaP}} - \mathrm{BE_{Si}}) \quad (1)$$

where $\mathrm{BE_{GaP}}$ and $\mathrm{BE_{Si}}$ are the binding energies of the respective core levels in GaP and Si and $\Delta E_{\mathrm{CoreLevel-Valence}}$ are the respective core level energy/valence band onsets differences shown in Fig. 2 at the example of Si. The valence band onset was obtained by performing a linear fit to the XPS valence band onset (see Fig. 2 inset). Three GaP core levels and one Si core level were measured so that three different combinations of binding energy differences were available to determine the valence band offset. Our study does not provide detailed information on the microscopic structure of the interface region such as intermediate phases. In general, the reduced binding energy at surfaces and interfaces can be different from the bulk case. Our results present an average of surface and bulk states and, hence, provide as a result the nanoscale band alignment without revealing the exact interface chemistry.

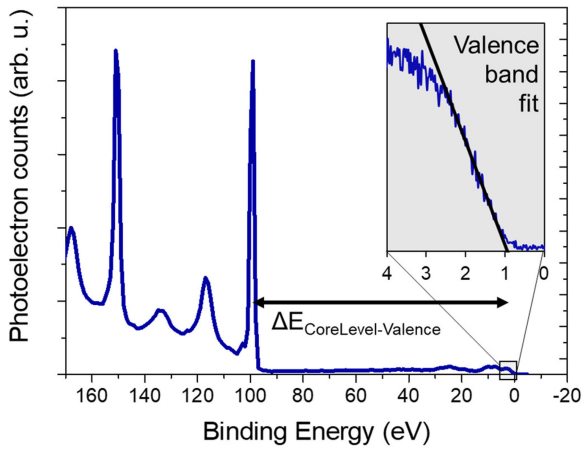

Fig. 2. XPS spectrum of silicon. The inset shows a magnification of the data in the binding energy interval 0–4 eV and a linear fit to the data for determination of the valence band onset.

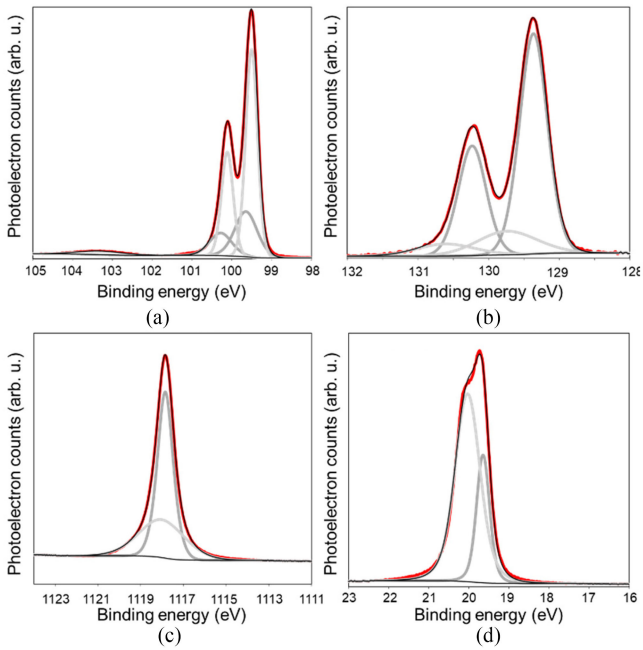

Fig. 3. Core-level spectra and fitting functions. (a) Si 2p. (b) P 2p. (c) Ga 2p (3/2). (d) Ga 3d.

In order to accurately determine the core-level positions, the XPS data were fitted using CASAXPS. A Shirley-type background was subtracted and peaks were fitted with Gaussian-Lorentzian line shapes. Constraints for the peak area were applied according to the spin-orbit splitting. Fig. 3 shows the measurement and components used for the fitting for (a) Si 2p, (b) P 2p, (c) Ga 2p (3/2), and (d) Ga 3d. The presented data are for pure Si (1 1 2) and Si (1 1 2) with 300-nm GaP. The red curves present the measured data, gray curves show the components that can be assigned to different element compositions and the black curves show the overall fit. The Si 2p signal is a superposition of elemental Si (main component, Si $2p_{3/2}$, and Si $2p_{1/2}$), SiC (second strongest signal, from adventitious C contamination), and SiO_2 at higher binding energy. The strongest

signal in the P and Ga spectra can be attributed to GaP bonds, while the weaker contribution results most likely from elemental Ga and P, respectively. The fitting parameters obtained from the thick materials were used in the fitting of interface measurements peaks such that weak signals were also fitted with high accuracy. We also investigated the influence of exposure to ambient air. The presented data were obtained after a brief exposure (5–20 min) to ambient air, and we can clearly see a SiO_2 signature at higher binding energy and a signal at the O 1 s binding energy (not shown here). After exposure to ambient air for several months, this signature becomes stronger but more importantly, additional peaks arise in the Ga and P spectrum that were not observed before (not shown here). Therefore, if native Ga or P oxide was present during our band alignment study, the signal was too low to be measured.

A further way to determine the valence band offset is by fitting the valence electron (low binding energy) spectra of GaP/Si samples as a linear superposition of the pure Si and the pure GaP [64]. This assumes that the measured signal at low binding energy of a thin layer on a substrate is composed of photoelectrons that were emitted from the valence bands of the thin layer and the substrate. It also assumes that the ratio of thin layer to substrate contribution remains constant within the whole energy regime that is investigated. This is a valid assumption as the escape depth for electrons with low binding energy and, therefore, kinetic energy >1 keV only weakly depends on the energy [65].

With these assumptions, the thin layer on substrate data can be modeled as a linear superposition of the pure elements' valence band spectra. For the superposition, the ratio of the contribution of the pure material spectra and the respective binding energy shift relative to the position of the valence band onset in the pure materials need to be determined. For Si, the valence band onset was at 0.8 ± 0.2 eV and the onset of the GaP valence band was at 1.38 ± 0.2 eV with respect to the Fermi level of the instrument. The binding energy shift can then be translated into the valence band offset of the two materials. We used an algorithm that minimized the sum of differences between linear combination and measured data to find the optimal parameters for the linear combination.

B. Cross-Sectional KPFM

An Asylum Research MFP-3D scanning probe microscope served as a KP and KPFM measurement system. Samples for cross-sectional KPFM were prepared by cleaving and mechanical polishing [66]. The polished side was made under an obtuse angle with respect to the grown surface to facilitate access with the cantilever. In all measurements, the Si substrates were connected to ground while the top layers were left on floating potential. The contact potential difference (CPD) [67] was applied to the probe. KPFM measurements were performed in dual-pass amplitude modulated mode and profiles were extracted from the 2-D images. Measurements were performed in the dark and under broadband illumination from an USHIO EKE 150 W halogen lamp coupled to a fiber bundle. The photovoltage was deduced as the difference of the CPD measured in the dark and under illumination [50].

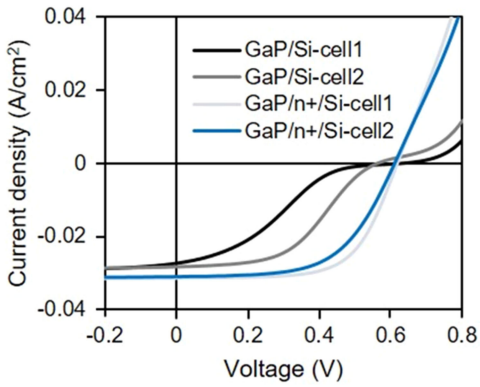

Fig. 4. Current–voltage characteristics of silicon heterojunction solar cells with material stack according to Fig. 1 with/without n+ doped Si layer at the GaP/Si interface for two different cells (cell1 and cell2), respectively.

IV. Results and Discussion

A. GaP/Si Heterojunction Solar Cell Device Characteristics

Current–voltage measurements were performed under 1-sun AM 1.5G illumination. We measured solar cells with and without n+ doped silicon at the GaP/Si interface. The results are shown in Fig. 4. With n+ doped silicon at the interface, we obtained a short-circuit current density of 31.3 ± 0.3 mA/cm^2, open-cicuit voltage of 616 ± 4 mV, fill factor of $61 \pm 4\%$, and efficiency of $11.8 \pm 1.0\%$. These values are in the same range as previous reports with similar device architecture [22], [24]. Without n+ doped silicon at the interface we obtained a short-circuit current density of 27.8 ± 0.7 mA/cm^2, open-circuit voltage of 595 ± 43 mV, fill factor of $36 \pm 2\%$, and efficiency of $5.9 \pm 2.2\%$. We measured charge carrier lifetime of more than 500 μs as published elsewhere [53]–[55]. This leads to an implied open-circuit voltage of greater than 650 mV [68], which shows that the open-circuit voltage was not limited by charge carrier recombination [69], but rather by the charge extraction. The trend of increased fill factor and open-circuit voltage upon introduction of n+ doped silicon has also been observed by other researchers [24].

One possible explanation for this behavior is a barrier for charge extraction at the GaP/Si interface. Therefore, we performed measurements that determine the band alignment between GaP and Si in our devices and we measured the photovoltage drop across the GaP/Si interface as presented in the following sections.

B. X-Ray Photoelectron Spectroscopy

Fig. 5 shows Si 2p, P 2p, Ga 2p (3/2), and Ga 3d core-level binding energy spectra of the thin films as well as the spectra of bare Si (1 1 2) and 300-nm GaP on Si (1 1 2) measured with the Kratos Ultra system. The thicker the GaP the more pronounced the Ga and P core-level peaks become, while the Si 2p peak becomes smaller. The thin films for the band alignment study were not doped intentionally, therefore, only minimal shift in peak position is observed for the GaP peaks which can be attributed to light n-doped background doping. The Si 2p peak on the other hand shifts toward higher binding energy for thicker

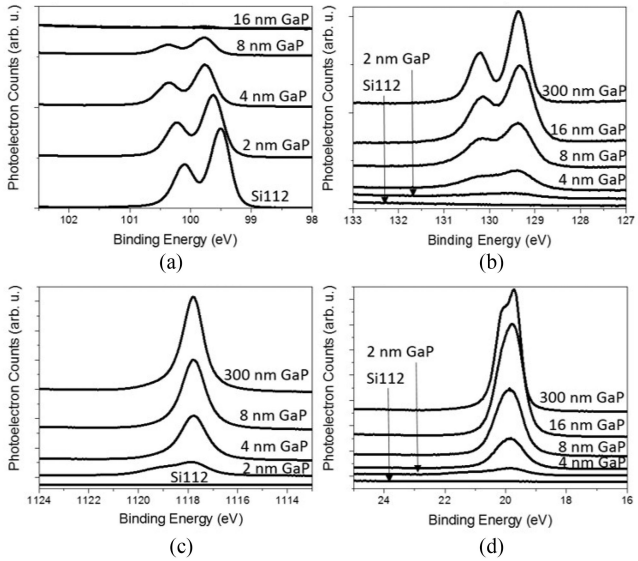

Fig. 5. XPS core-level spectra of GaP grown by MOCVD on Si (1 1 2).

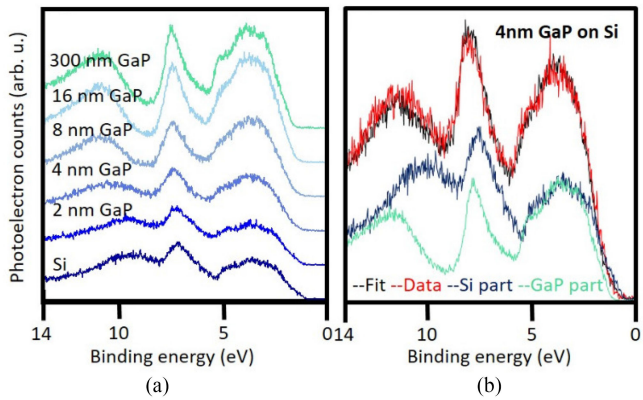

Fig. 6. (a) Valence band spectrum measured by XPS of Si and Si/GaP with varying GaP thickness grown by MOCVD. (b) Example fit of a combined GaP/Si valence spectrum as the superposition of Si and GaP valence spectra.

GaP that corresponds to downward bending of the valence band. The Si (1 1 2) wafers were slightly p-doped (10^{12} 1/cm^3) such that silicon band bending would be expected but, moreover, the initial shift of the Si 2p peak could be a result of gap state introduction and subsequent Fermi-level pinning caused by the GaP deposition. Furthermore, it should be noted that we cannot ensure that the thin layers fully cover the silicon and that island growth might not be present.

The core-level spectra were fitted as a superposition of the involved materials in order to quantify the peak positions. For the calculations, Si 2p 3/2, Ga 2p 3/2, P 2p 3/2, and Ga 3d 5/2 were used, respectively. Applying (1) to all measurements led to an average valence band offset of 0.22 $\pm$ 0.12 eV for the MOCVD grown samples and 0.30 $\pm$ 0.17 eV for MBE grown samples. No systematic difference between the valence band offset of GaP grown on Si (1 1 2) and Si (0 0 1) was observed.

It can be seen that for the thinnest GaP layer (2 nm), a "shoulder" is observed toward higher binding energy for the Ga 3d and the Ga 2p (3/2). In order to fit this data properly, a new component needs to be introduced that would suggest an additional chemical bond of the Ga that is only observable when measuring a very thin layer. This effect cannot be observed for the P 2p, Si 2p, and Ga 3d peak. It needs to be noted that the Ga 2p (3/2) peak provides a 3–8 times higher photoelectron count and, therefore, significantly better signal-to-noise ratio than the other core-level peaks such that it is expected for an additional bond to become first visible at the Ga 2p (3/2) core level. An additional Ga bond would suggest a Ga-Si layer at the interface. This is in accordance with the observation by Supplie *et al.* [38] that without proper cleaning or preconditioning of the reactor Ga and P species are present due to outgassing from the reactor walls. They showed that Ga–Si bonds form at the interface even before the initial growth pulse. Cleaning and conditioning were not performed on the MBE and MOCVD chambers before growth. Therefore, it is reasonable that in both the MOCVD and MBE growth, Si–Ga bonds determine the observed band alignment.

Fig. 6(a) shows the low-binding energy XPS spectra of Si (1 1 2) with 2, 4, 8, 16, and 300-nm GaP. The Si valence band spectrum resembles previously measured spectra [70], [71]. The spectra of very thin layers can be described as a linear combination of the bare Si spectrum and the 300-nm GaP spectrum [64]. We used an algorithm that minimized the sum of differences between linear combination and measured data to find the optimal parameters for the linear combination. The important parameters are the ratios of the thick level spectra and their energy shifts. In the presented case, the Si:GaP ratio is the following: 95:7 for 2-nm GaP, 69:30 for 4-nm GaP, 28:71 for 8-nm GaP, and 3:103 for 16-nm GaP. It can be seen that the ratio changes toward higher GaP content for thicker GaP layers. This is expected as lesser the photoelectrons escape from the Si, the thicker the GaP layer. Fig. 6(b) shows the results of a fitting procedure for a measurement on a sample with 4-nm GaP on Si. An accurate fit for this superposition is achieved with a ratio of Si to GaP of 69:30. The Si spectrum needs to be shifted by 0.1 eV and the GaP spectrum is shifted by –0.2 eV. Performing this fitting procedure with the spectra obtained from all measurements, we obtained an average valence band offset of 0.29 $\pm$ 0.14 eV. All presented XPS results were reproduced with different samples, different air exposure time, and on two different XPS instruments. We measured a mean valence band offset of 0.24 $\pm$ 0.12 eV out of 56 measurements for the MOCVD grown samples that were exposed to air for less than 10 min. With an ambient air exposure of several weeks, the value increased to 0.40 $\pm$ 0.12 eV. One batch of MBE grown samples was also investigated by XPS in order to make sure that the observed characteristics of MBE-grown devices can actually be attributed to the high conduction band offset. For these samples, we obtained a mean valence band offset of 0.30 $\pm$ 0.17 eV. All results are presented in Table I. One data point is significantly higher (1.54 eV) than the others which we attribute to poor signal-to-noise-ratio due to the weak GaP valence band signal for very thin layers. Therefore, we can conclude that for MBE as well as for MOCVD grown samples,

TABLE I
BAND OFFSET RESULTS DETERMINED BY XPS

Subs.	Growth	d	Instr.	Val.	Ga 2p	P 2p	Ga 3d
Si001	MOCVD	2	Kratos	1.54	0.34	0.31	0.19
Si001	MOCVD	4	Kratos	0.49	0.24	0.20	0.13
Si001	MOCVD	8	Kratos	0.21	0.26	0.18	0.14
Si001	MOCVD	16	Kratos	0.14	0.13	0.03	0.01
Si001	MOCVD	4	MProb		0.20	0.35	0.26
Si001	MOCVD	8	MProb		0.12	0.21	0.17
Si001	MBE	5	Kratos		0.28	0.31	0.30
Si112	MOCVD	2	Kratos	0.19	0.32	0.42	0.29
Si112	MOCVD	4	Kratos	0.44	0.27	0.19	0.15
Si112	MOCVD	8	Kratos	0.34	0.25	0.16	0.20
Si112	MOCVD	16	Kratos	0.39		0.15	0.16
Si112	MOCVD	2	Kratos	0.34	0.35	0.22	0.22
Si112	MOCVD	4	Kratos	0.44	0.26	0.18	0.17
Si112	MOCVD	8	Kratos	0.11	0.27	0.18	0.18
Si112	MOCVD	16	Kratos	0.11	0.21	0.10	0.10
Si112	MOCVD	2	Kratos			0.44*	0.43*
Si112	MOCVD	4	Kratos			0.39*	0.34*

Subs.: Substrate; d: layer thickness in nm; Val.: valence band offset in eV determined by fitting of the valence band; Ga 2p, P 2p, and Ga 3d: valence band offset in eV obtained by the core level energy difference between Si 2p and the respective GaP core level. *Sample was stored in ambient air for several weeks before the XPS measurement.

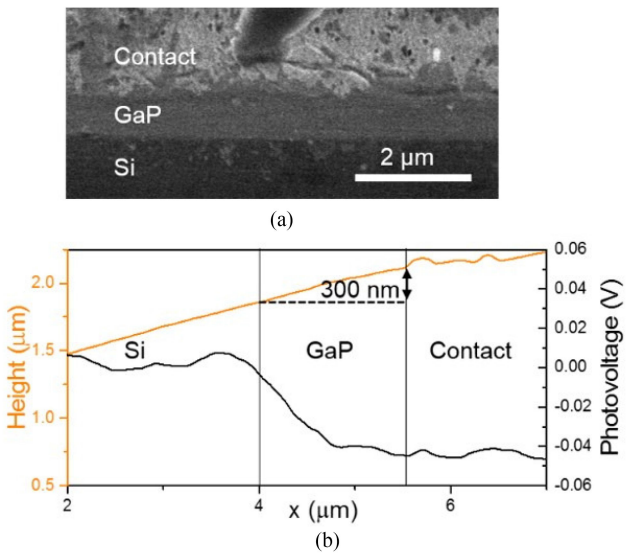

Fig. 7. (a) SEM image of the cross section. (b) Height and photovoltage profile across the cross section.

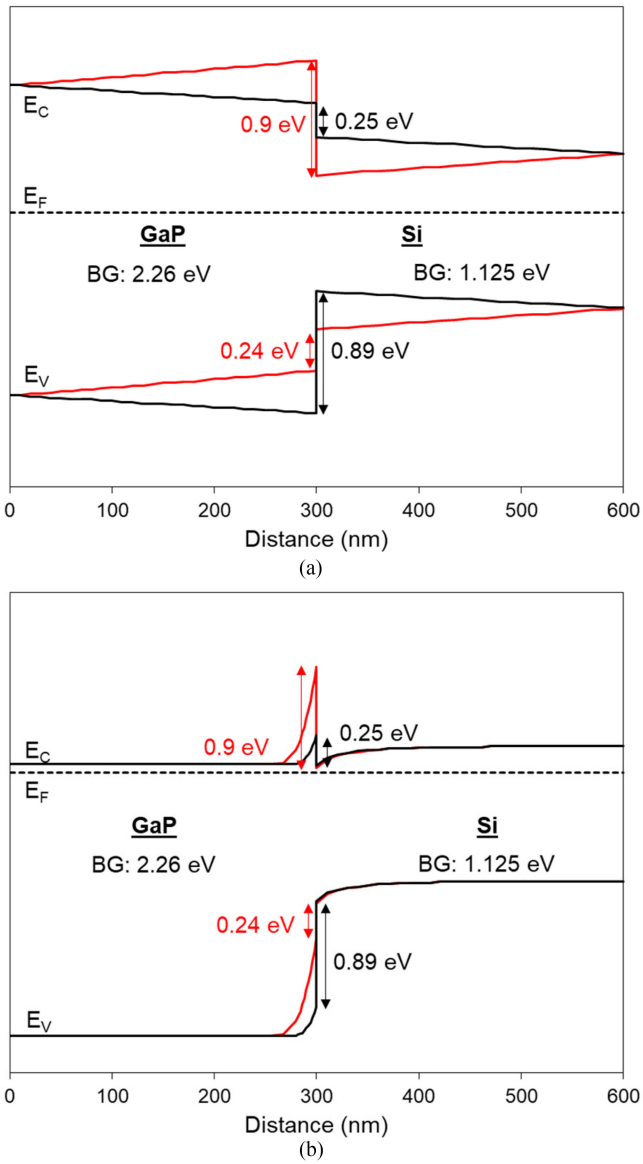

Fig. 8. Band diagram for the doping level used. (a) XPS analysis. (b) Solar cell devices as measured (red) and as predicted by Anderson's rule (black). Band diagrams were calculated using AFORS-HET v2.4.1.

the conduction band offset is significantly greater than predicted by Anderson's rule.

C. Cross-Sectional KP Force Microscopy

The results of a cross-sectional KPFM measurement are presented in Fig. 7. Fig. 7(a) shows a scanning electron microscopy image of the investigated cross section. Residues from the polishing can be observed in the silicon region. For scanning probe measurements, a location without residues was used in order to avoid measurement artifacts. The GaP was grown by MOCVD. In Fig. 7, the topography (orange) as well as the photovoltage (black) profile across the cross section are shown for a region with an ohmic Ni/Au/Ge/Au contact [72]. Using the height profile, the different layers were identified. The photovoltage drops along the depletion zone between Si and GaP as can be seen in Fig. 7(b). This shows that the depletion zone acts as the major charge transport barrier within the observed region and shows that the top contact provides ohmic behavior. It has been shown before in a cross-sectional KPFM study that S-shaped current voltage characteristics can be correlated with barriers at contact layers [31]. Therefore, the cross-sectional KPFM measurements fortify our XPS band alignment measurements that revealed high conduction band offset and, therefore, a high charge transport barrier for electrons in the case of low doping levels in the Si and GaP.

V. Band-Alignment at the GaP/Si Interface

The band alignment was calculated using the heterostructure simulator AFORS-HET v2.4.1 [73] with the Si and GaP doping levels used in the XPS measurements (a) and in the solar cell devices (b). Band gap (BG) [74] and electron affinity [16] values were taken from the literature. Without including an interface dipole, AFORS-HET calculates a valence band offset of 0.89 eV and a conduction band offset of 0.25 eV as predicted by Anderson's rule. This small conduction band offset of 0.25 eV would not hinder charge transport [75] and the resulting band diagram is consistent with a similar study by Zelentsov and Gudovskikh [76]. However, when including an interface dipole, we obtain the red band alignment. In AFORS-HET, this was realized by changing the electron affinity of GaP to 3.21 eV. This results in a significantly increased tunnel barrier at the GaP/Si interface, which constitutes a barrier for charge transport as confirmed by our cross-sectional KPFM measurements. Note that we did not explicitly investigate the charge extraction from the GaP into the ITO, which can have additional effects on the solar cell characteristics. The presented band alignment diagram presents one possible explanation for the discrepancy between the theoretically predicted and measured device characteristics of GaP/Si heterojunction solar cells.

VI. Conclusion

We have performed band alignment measurements at the GaP/Si interface for silicon heterojunction solar cells. Contrary to theoretical predictions using the Anderson model, we found a very low-valence band offset (0.24 ± 0.12 eV) and, therefore, a very high (0.9 eV) conduction band offset leading to a barrier for electron transport. Our solar cells exhibit low fill factor or even S-shaped current–voltage characteristics. The fill factor can be increased by highly n-doping the Si at the GaP/Si interface as also observed by others [24]. We performed cross-sectional KPFM measurements [49]–[51] that revealed a strong photovoltage drop at the GaP/Si interface. Altogether, these findings suggest a charge transport barrier at the interface between Si and GaP—caused by unfavorable band alignment—being the culprit of poor GaP/Si heterojunction solar cell performance.

Recently, experimental studies on GaP/Si heterojunction solar cells have been performed, and in all cases open-circuit voltages are surprisingly low [22], [54]. With reported minority charge carrier lifetime greater than 100 μs, the open-circuit voltage is not limited by surface recombination [69], and a barrier for charge carrier extraction is one likely explanation. The band alignment depends strongly on the substrate surface [45], the growth conditions [34], [45], and the reactor cleanliness [34], [38]. From our XPS data and previous studies [34], [38], it is likely that the band alignment is determined by Si–Ga bonds present at the interface. In particular, our observation of similar band alignment for growth with MBE as well as MOCVD suggests that the same mechanism is the culprit. We did not clean or coat our reactor with pristine materials which according to Supplie *et al.* [38] leads to Si–Ga bonds at the interface due to outgassing from the reactor walls. Furthermore, a study by Beyer *et al.* suggests that the poor decomposition of TBP in the MOCVD growth also favors Si–Ga bonds [61]. Therefore, in conjunction with our XPS results showing the presence of Si–Ga bonds at the interface, the observed behavior can be explained by an interface dipole caused by a Ga-rich interface. An *ab initio* density functional theory study on the atomic and electronic structure of GaP/Si(0 0 1) heterointerfaces by Romanyuk *et al.* [44] predicts the valence band offset to be 0.32 eV for an abrupt Si–Ga interface which is within the confidence interval of this study. This also offers a microscopic explanation for the significantly lower valence band offset than observed in XPS studies performed at the GaP/Si interface in the 1980s [32], [33], [39], [40].

In summary, our study offers an explanation for the observed characteristics of GaP/Si heterojunction solar cells which is consistent with recent experimental and theoretical studies. It demonstrates that close attention has to be paid to the interface properties in order to increase open-circuit voltage and fill factor GaP/Si heterojunction solar cells.

Acknowledgment

The authors would like to thank the Molecular Foundry for generously hosting the MOCVD growth and the Caltech MMRC for providing the XPS analytic tools and also L. Ding, S. Aloni, A. Nielander, N. Plymale, A. Shing, and L. Korte for helpful advice with measurements and data interpretation.

References

[1] K. Yoshikawa *et al.*, "Silicon heterojunction solar cell with interdigitated back contacts for a photoconversion efficiency over 26%," *Nature Energy*, vol. 2, 2017, Art. no. 17032.

[2] M. Tanaka *et al.*, "Development of new a-Si/c-Si heterojunction solar cells: ACJ-HIT (artificially constructed junction-heterojunction with intrinsic thin-layer)," *Jpn. J. Appl. Phys.*, vol. 31, 1992, Art. no. 3518.

[3] A. Cuevas, A. Luque, J. Eguren, and J. Del Alamo, "50 Per cent more output power from an albedo-collecting flat panel using bifacial solar cells," *Solar Energy*, vol. 29, pp. 419–420, 1982.

[4] T. C. Russell, R. Saive, A. Augusto, S. G. Bowden, and H. A. Atwater, "The influence of spectral albedo on bifacial solar cells: A theoretical and experimental study," *IEEE J. Photovol.*, vol. 7, no. 6, pp. 1611–1618, Nov. 2017.

[5] M. Boccard and Z. C. Holman, "Amorphous silicon carbide passivating layers for crystalline-silicon-based heterojunction solar cells," *J. Appl. Phys.*, vol. 118, 2015, Art. no. 065704.

[6] C. Battaglia *et al.*, "Silicon heterojunction solar cell with passivated hole selective MoOx contact," *Appl. Phys. Lett.*, vol. 104, 2014, Art. no. 113902.

[7] R. Saive *et al.*, "Effectively transparent contacts (ETCs) for solar cells," in *Proc. IEEE 43rd Photovol. Specialists Conf.*, 2016, pp. 3612–3615.

[8] R. Saive *et al.*, "Effectively transparent front contacts for optoelectronic devices," *Adv. Opt. Mater.*, vol. 4, pp. 1470–1474, 2016.

[9] R. Saive *et al.*, "Silicon heterojunction solar cells with effectively transparent front contacts," *Sustain. Energy Fuels*, vol. 1, pp. 593–598, 2017.

[10] Z. C. Holman *et al.*, "Current losses at the front of silicon heterojunction solar cells," *Photovol. IEEE J.*, vol. 2, no. 1, pp. 7–15, Jan. 2012.

[11] J. Bullock *et al.*, "Efficient silicon solar cells with dopant-free asymmetric heterocontacts," *Nature Energy*, vol. 1, 2016, Art. no. 15031.

[12] J. Bullock, A. Cuevas, T. Allen, and C. Battaglia, "Molybdenum oxide MoOx: A versatile hole contact for silicon solar cells," *Appl. Phys. Lett.*, vol. 105, 2014, Art. no. 232109.

[13] M. Feifel *et al.*, "Gallium phosphide window layer for silicon solar cells," *IEEE J. Photovol.*, vol. 6, no. 1, pp. 384–390, Jan. 2016.

[14] C. T Chen, R. Saive, H. Emmer, S. Aloni, and H. A. Atwater, "GaP/Si heterojunction solar cells," in *Proc. 42nd IEEE Photovol. Specialist Conf.*, 2015, pp. 1–3.

[15] M. Lorenz, G. Pettit, and R. Taylor, "Band gap of gallium phosphide from 0 to 900 k and light emission from diodes at high temperatures," *Phys. Rev.*, vol. 171, 1968, Art. no. 876.

[16] M. S. Shur, *Handbook Series on Semiconductor Parameters*, vol. 1, Singapore: World Scientific, 1996.

[17] H. Wagner *et al.*, "A numerical simulation study of gallium-phosphide/silicon heterojunction passivated emitter and rear solar cells," *J. Appl. Phys.*, vol. 115, 2014, Art. no. 044508.

[18] F. Himpsel, G. Hollinger, and R. Pollak, "Determination of the Fermi-level pinning position at Si (111) surfaces," *Phys. Rev. B*, vol. 28, 1983, Art. no. 7014.

[19] J. Tersoff, "Schottky barrier heights and the continuum of gap states," *Phys. Rev. Lett.*, vol. 52, 1984, Art. no. 465.

[20] J. Tersoff, "Theory of semiconductor heterojunctions: The role of quantum dipoles," *Phys. Rev. B*, vol. 30, 1984, Art. no. 4874.

[21] R. T. Tung, "Recent advances in Schottky barrier concepts," *Mater. Sci. Eng., R.*, vol. 35, pp. 1–138, 2001.

[22] T. Grassman *et al.*, "MOCVD-grown GaP/Si subcells for integrated III–V/Si multijunction photovoltaics," *IEEE J. Photovol.*, vol. 4, pp. 972–980, 2014.

[23] J. I. Deitz, D. W. McComb, and T. J. Grassman, "Probing the electronic structure at the heterovalent GaP/Si interface using electron energy-loss spectroscopy," in *Proc. IEEE 41st Photovol. Specialists Conf.*, 2016, pp. 1545–1548.

[24] M. Feifel *et al.*, "MOVPE grown gallium phosphide–silicon heterojunction solar cells," *IEEE J. Photovol.*, vol. 7, no. 2, pp. 502–507, Mar. 2017.

[25] P. Muralidharan, S. Bowden, S. M. Goodnick, and D. Vasileska, "A multi-scale modeling approach to study transport in silicon heterojunction solar cells," *Additional Papers Presentations*, vol. 2016, pp. 002095–002110, 2016.

[26] P. Luppina, S. Bowden, P. Lugli, and S. M. Goodnick, "Modeling of a gallium phosphide/silicon heterojunction solar cells," in *Proc. IEEE 43rd Photovol. Specialists Conf.*, 2016, pp. 2467–2472.

[27] E. Centurioni, D. Iencinella, R. Rizzoli, and F. Zignani, "Silicon heterojunction solar cell: A new buffer layer concept with low-temperature epitaxial silicon," *IEEE Trans. Electron Devices*, vol. 51, no. 11, pp. 1818–1824, Nov. 2004.

[28] U. Das *et al.*, "Investigation of hetero-interface and junction properties in silicon heterojunction solar cells," in *Proc. IEEE 35th Photovolt. Specialists Conf.*, 2010, pp. 001358–001362.

[29] M. Lu, U. Das, S. Bowden, S. Hegedus, and R. Birkmire, "Optimization of interdigitated back contact silicon heterojunction solar cells: Tailoring hetero-interface band structures while maintaining surface passivation," *Progress Photovolt., Res. Appl.*, vol. 19, pp. 326–338, 2011.

[30] A. Gudovskikh, J.-P. Kleider, A. Froitzheim, W. Fuhs, and E. Terukov, "Investigation of a-Si: H/c-Si heterojunction solar cells interface properties," *Thin Solid Films*, vol. 451, pp. 345–349, 2004.

[31] R. Saive, C. Mueller, J. Schinke, R. Lovrincic, and W. Kowalsky, "Understanding S-shaped current-voltage characteristics of organic solar cells: Direct measurement of potential distributions by scanning Kelvin probe," *Appl. Phys. Lett.*, vol. 103, 2013, Art. no. 243303.

[32] D. W. Niles and H. Höchst, "Electronic structure of the Si/GaP (110) interface," *Phys. Rev. B*, vol. 39, 1989, Art. no. 7769.

[33] P. Perfetti *et al.*, "Experimental study of the GaP-Si interface," *Phys. Rev. B*, vol. 30, 1984, Art. no. 4533.

[34] O. Supplie *et al.*, "Time-resolved in situ spectroscopy during formation of the GaP/Si (100) heterointerface," *J. Phys. Chem. Lett.*, vol. 6, pp. 464–469, 2015.

[35] K. Ishioka *et al.*, "Coherent phonon spectroscopy characterization of electronic bands at buried semiconductor heterointerfaces," *Appl. Phys. Lett.*, vol. 108, 2016, Art. no. 051607.

[36] I. Sakata and H. Kawanami, "Band discontinuities in gallium phosphide/crystalline silicon heterojunctions studied by internal photoemission," *Appl. Phys. Express*, vol. 1, 2008, Art. no. 091201.

[37] R. Roychowdhury *et al.*, "Role of surface energy on the morphology and optical properties of GaP micro & nano structures grown on polar and non-polar substrates," *Appl. Surface Sci.*, vol. 419, pp. 957–967, 2017.

[38] O. Supplie *et al.*, "Formation of GaP/Si (100) heterointerfaces in the presence of inherent reactor residuals," *ACS Appl. Mater. Interfaces*, vol. 7, pp. 9323–9327, 2015.

[39] P. Perfetti *et al.*, "Parallel measurements of both heterojunction band discontinuities by synchrotron-radiation photoemission," *Phys. Rev. B*, vol. 29, 1984, Art. no. 5941.

[40] A. Katnani and G. Margaritondo, "Microscopic study of semiconductor heterojunctions: photoemission measurement of the valance-band discontinuity and of the potential barriers," *Phys. Rev. B*, vol. 28, 1983, Art. no. 1944.

[41] C. Calandra, F. Manghi, and C. Bertoni, "Theoretical study of the electronic structure of the GaP (110)□ Si interface," *Surface Sci.*, vol. 162, pp. 605–609, 1985.

[42] M. Lazzouni, M. Peressi, and A. Baldereschi, "Valence-band offset at the Si/GaP (110) interface," *Appl. Phys. Lett.*, vol. 68, pp. 75–77, 1996.

[43] R. Dandrea, S. Froyen, and A. Zunger, "Stability and band offsets of heterovalent superlattices: Si/GaP, Ge/GaAs, and Si/GaAs," *Phys. Rev. B*, vol. 42, 1990, Art. no. 3213.

[44] O. Romanyuk, O. Supplie, T. Susi, M. May, and T. Hannappel, "Ab initio density functional theory study on the atomic and electronic structure of GaP/Si (001) heterointerfaces," *Phys. Rev. B*, vol. 94, 2016, Art. no. 155309.

[45] T. Grassman *et al.*, "Nucleation-related defect-free GaP/Si (100) heteroepitaxy via metal-organic chemical vapor deposition," *Appl. Phys. Lett.*, vol. 102, 2013, Art. no. 142102.

[46] L. Kelvin, "V. Contact electricity of metals," *The London, Edinburgh, Dublin Philosophical Mag. J. Sci.*, vol. 46, pp. 82–120, 1898.

[47] R. Shikler, T. Meoded, N. Fried, and Y. Rosenwaks, "Potential imaging of operating light-emitting devices using Kelvin force microscopy," *Appl. Phys. Lett.*, vol. 74, pp. 2972–2974, 1999.

[48] V. W. Bergmann *et al.*, "Real-space observation of unbalanced charge distribution inside a perovskite-sensitized solar cell," *Nature Commun.*, vol. 5, 2014, Art. no. 5001.

[49] R. Saive *et al.*, "Imaging the electric potential within organic solar cells," *Adv. Functional Mater.*, vol. 23, pp. 5854–5860, 2013.

[50] R. Saive, "Investigation of the potential distribution within organic solar cells by scanning Kelvin probe microscopy," 2014.

[51] C. S. Weigel, W. Kowalsky, and R. Saive, "Direct observation of the potential distribution within organic light emitting diodes under operation," *Phys. Status Solidi Rapid Res. Lett.*, vol. 9, no. 8, pp. 475–479, 2015.

[52] S. L. Wright, H. Kroemer, and M. Inada, "Molecular beam epitaxial growth of GaP on Si," *J. Appl. Phys.*, vol. 55, pp. 2916–2927, 1984.

[53] L. Ding *et al.*, "On the source of silicon minority-carrier lifetime degradation during molecular beam heteroepitaxial growth of III-V materials," in *Proc. IEEE 43rd Photovolt. Specialists Conf.*, 2016, pp. 2048–2051.

[54] C. Zhang *et al.*, "Hetero-emitter GaP/Si solar cells with high Si bulk lifetime," in *Proc. IEEE 43rd Photovolt. Specialists Conf.*, 2016, pp. 1950–1953.

[55] C. Zhang, Y. Kim, N. N. Faleev, and C. B. Honsberg, "Improvement of GaP crystal quality and silicon bulk lifetime in GaP/Si heteroepitaxy," *J. Crystal Growth*, vol. 475, pp. 83–87, 2017.

[56] L. Ding *et al.*, "Silicon minority-carrier lifetime degradation during molecular beam heteroepitaxial III-V material growth," *Energy Procedia*, vol. 92, pp. 617–623, 2016.

[57] H. Kroemer, "Polar-on-nonpolar epitaxy," *J. Crystal Growth*, vol. 81, pp. 193–204, 1987.

[58] C. T. Chen, "Heteroepitaxy of group IV and group III-V semiconductor alloys for photovoltaic applications," California Instit. Technol., Pasadena, CA, USA, 2016.

[59] H. Emmer *et al.*, "Fabrication of single crystal gallium phosphide thin films on glass," *Sci. Rep.*, vol. 7, 2017, Art. no. 4643.

[60] K. Volz *et al.*, "GaP-nucleation on exact Si (001) substrates for III/V device integration," *J. Crystal Growth*, vol. 315, pp. 37–47, 2011.

[61] A. Beyer *et al.*, "GaP heteroepitaxy on Si (001): Correlation of Si-surface structure, GaP growth conditions, and Si-III/V interface structure," *J. Appl. Physics*, vol. 111, 2012, Art. no. 083534.

[62] E. García-Tabarés *et al.*, "Evolution of silicon bulk lifetime during III–V-on-Si multijunction solar cell epitaxial growth," *Progress Photovolt., Res. Appl.*, vol. 24, pp. 634–644, 2015.

[63] E. Kraut, R. Grant, J. Waldrop, and S. Kowalczyk, "Precise determination of the valence-band edge in x-ray photoemission spectra: Application to measurement of semiconductor interface potentials," *Phys. Rev. Lett.*, vol. 44, 1980, Art. no. 1620.

[64] L. Korte, R. Rößler, and C. Pettenkofer, "Direct determination of the band offset in atomic layer deposited ZnO/hydrogenated amorphous silicon heterojunctions from X-ray photoelectron spectroscopy valence band spectra," *J. Appl. Phys.*, vol. 115, 2014, Art. no. 203715.

[65] M. P. Seah and W. Dench, "Quantitative electron spectroscopy of surfaces: A standard data base for electron inelastic mean free paths in solids," *Surface Interface Anal.*, vol. 1, pp. 2–11, 1979.

[66] M. Scherer, R. Saive, D. Daume, M. Kröger, and W. Kowalsky, "Sample preparation for scanning Kelvin probe microscopy studies on cross sections of organic solar cells," *AIP Adv.*, vol. 3, 2013, Art. no. 092134.
[67] D. Cahen and A. Kahn, "Electron energetics at surfaces and interfaces: concepts and experiments," *Adv. Mater.*, vol. 15, pp. 271–277, 2003.
[68] R. Sinton and A. Cuevas, "A quasi-steady-state open-circuit voltage method for solar cell characterization," in *Proc. 16th Eur. Photovolt. Solar Energy Conf.*, vol. 1152, 2000.
[69] R. A. Sinton and A. Cuevas, "Contactless determination of current–voltage characteristics and minority-carrier lifetimes in semiconductors from quasi-steady-state photoconductance data," *Appl. Phys. Lett.*, vol. 69, pp. 2510–2512, 1996.
[70] L. Ley, S. Kowalczyk, R. Pollak, and D. Shirley, "X-ray photoemission spectra of crystalline and amorphous Si and Ge valence bands," *Phys. Rev. Lett.*, vol. 29, 1972, Art. no. 1088.
[71] R. Puthenkovilakam and J. P. Chang, "Valence band structure and band alignment at the ZrO 2/Si interface," *Appl. Phys. Lett.*, vol. 84, pp. 1353–1355, 2004.
[72] M. Islam and P. J. McNally, "A comparative study of Pd/Sn/Au, Au/Ge/Au/Ni/Au, Au-Ge/Ni and Ni/Au-Ge/Ni ohmic contacts to n-GaAs," *Microelectron. Eng.*, vol. 40, pp. 35–42, 1998.
[73] R. Varache *et al.*, "Investigation of selective junctions using a newly developed tunnel current model for solar cell applications," *Solar Energy Mater. Solar Cells*, vol. 141, pp. 14–23, 2015.
[74] "Gallium phosphide (GaP), indirect band gaps," Datasheet from Landolt-Börnstein – Group III Condensed Matter. Volume 41A1β: in Group IV Elements, IV-IV and III-V Compounds. Part b – Electronic, Transport, Optical and Other Properties O. Madelung, U. Rössler, and M. Schulz, Eds. Berlin, Germany: Springer-Verlag, doi: 10.1007/10832182_136.
[75] H. S. Emmer, "Paths towards high efficiency silicon photovoltaics," California Instit. Technol., Pasadena, CA, USA, 2016.
[76] K. Zelentsov and A. Gudovskikh, "GaP/Si anisotype heterojunction solar cells," *J. Phys., Conf. Series*, vol. 741, 2016, Art. no. 012096.

Authors' photographs and biographies not available at the time of publication.